# Synthesis and Characterization of Novel V/O/$SO_4$ Chains Incorporating 2,2′-Bipyridine Ligands: Crystal Structure of $[V_2O_2(OH)_2(SO_4)(2,2'\text{-bpy})_2]$

**M. Ishaque Khan,*,† Sabri Cevik,† Douglas Powell,‡ Sichu Li,§ and Charles J. O'Connor§**

Department of Biological, Chemical, and Physical Sciences, Illinois Institute of Technology, Chicago, Illinois 60616, Department of Chemistry, University of Wisconsin, Madison, Wisconsin 53706, and Department of Chemistry, University of New Orleans, New Orleans, Louisiana 70148

*Received August 1, 1997*

The hydrothermal reaction of a mixture of vanadyl acetylacetonate ($VO(acac)_2$), $Na_2SO_4$, 2,2′-bipyridine (2,2′-bpy), and $H_2O$ for 48 h at 160 °C gives brown crystals of $[V_2O_2(OH)_2(SO_4)(2,2'\text{-bpy})_2]$ (**1**) in 70% yield. The structure of **1** consists of ribbons constructed from the infinite inorganic chains, $[-\{V_2O_2(OH)_2\}-\mu_2\text{-}SO_4\{V_2O_2(OH)_2\}-SO_4]_\infty$, incorporating organic (2,2′-bipyridine) ligands. The inorganic chains are composed of the pairs of edge-sharing octahedra joined by $\{SO_4\}$ tetrahedra through octahedral−tetrahedral corner sharing. The octahedral geometry around each vanadium(IV) ion is defined by $\{VO_2(OH)_2N_2\}$ with each $V^{IV}$ center coordinated to a terminal oxo group, two $\mu_2$-OH groups, two nitrogen donor atoms from a chelating 2,2′-bipyridine ligand, and an oxygen donor atom from a $\mu_2$-$SO_4^{2-}$ ligand. Crystal data for **1**: monoclinic space group $P2_1/n$ (No. 14), $a = 11.7937(2)$ Å, $b = 12.1161(3)$ Å, $c = 15.5763(2)$ Å, $\beta = 93.750(2)°$, $Z = 4$. **1** constitutes the first example of a fully reduced vanadosulfate ($V/O/SO_4$) based solid incorporating both the organic and inorganic ligands. The novel solid exhibits Curie−Weiss paramagnetism at high temperature ($T > 140$ K) and short-range antiferromagnetic coupling between the $V^{IV}$ centers at lower temperature.

## Introduction

The intense current interest in synthetic inorganic materials[1] is a major driving force behind the significant efforts directed toward the design and development of synthetic strategies[2] for systems with novel structural and topological properties. Many organic molecules have been employed to direct the synthesis of complex organized structures of new materials exhibiting promising sorbent and catalytic activities.[3] Organic ligands have been used in intercalation systems and for linking metal centers to generate extended structures with channels and large cavities.[3b,4] On the other hand, an impressive array of inorganic oxometallic phosphate phases, composed of oxometalate polyhedra and phosphate tetrahedral units, exhibiting fascinating structural, electronic,[5,6] [1b,2b] and microporous[7] properties have been prepared by combining the versatile inorganic phosphate ligand with suitable transition metal ion precursors. Several well-characterized oxometallophosphates, organophosphonates, and organoarsonates, encapsulating and/or incorporating alkylamines, alkenediamines, and bipyridine etc., have also been reported in recent years.[3b,8−11]

There has been, however, considerable paucity in the development of oxometallic sulfate systems. Few fragmentary reports[12−19] on the solids and discrete molecular species composed of oxometallic polyhedra and sulfate tetrahedra are focused on the possible catalytic role of $V/O/SO_4$ compounds in the industrial production of sulfuric acid[12,13] and on solid

* Corresponding author.
† Illinois Institute of Technology.
‡ University of Wisconsin.
§ University of New Orleans.

(1) (a) Bruce, D. W.; O'Hare, D. *Inorganic Materials;* John Wiley & Sons: New York, 1992. (b) Suib, S. L. *Chem. Rev.* **1993**, *93*, 803.
(2) (a) Mallouk,T. E.; Lee, H. *J. Chem. Educ*. **1990**, *67*, 829. (b) Stein, A.; Keller, S. W.; Mallouk, T. E. *Science* (*Washington, D.C.*), **1993**, *259*, 1558. (c) Gopalakrishnan, J. *Chem. Mater*. **1995**, *7*, 1265. (d) *Supramolecular Architecture: Synthetic Control in Thin Films and Solids*; Bein, T., Ed.; ACS Symposium Series 499; American Chemical Society: Washington, DC, 1992.
(3) (a) Davis, M. E. *Cattech* **1997**, *1*, 19. (b) Schöllhorn, R. *Chem. Mater*. **1996**, *8*, 1747. (c) Raman, N. K.; Anderson, M. T.; Brinker, C. J. *Chem. Mater*. **1996**, *8*, 1683.
(4) (a) Yaghi, O. M.; Li, G. *Angew. Chem., Int. Ed. Engl.* **1995**, *34*, 207. (b) Fujita, M.; Kwon, Y. J.; Washizu, S.; Ogura, K. *J. Am. Chem. Soc.* **1994**, *116*, 1151. (c) Robson, R.; Abrahams, B. F.; Batten, S. R.; Gable, R. W.; Hoskins, B. F.; Liu, J. In *Supramolecular Architecture: Synthetic Control in Thin Films and Solids;* Bein, T.; Ed.; ACS Symposium Series 499; American Chemical Society: Washington, DC, 1992.
(5) (a) Haushalter, R. C.; Mundi, L. *Chem. Mater*. **1992**, *4*, 31. (b) Haushalter, R. C.; Meyer, L. M.; Zubieta, J. In *Early Transition Metal Clusters With* Π*-Donor Ligands*; Chisholm, M. H., Ed.; VCH: New York, 1995.
(6) Canadell, E.; Provost, J.; Guesdon, A.; Borel, M. M.; Leclaire, A. *Chem. Mater*. **1997**, *9*, 68.
(7) (a) Haushalter, R. C.; Strohmaier, K.; Lai, F. *Science* (*Washington, D.C.*) **1989**, *246*, 1289. (b) Chen, J.; Jones, R.; Natarajan, S.; Hursthouse, M. B.; Thomas, J. M. *Angew. Chem., Int. Ed. Engl*. **1994**, *33*, 639. (c) Hoelscer, M.; Englert, U.; Zibrowius, B.; Hoelderich, W. *Angew. Chem., Int. Ed. Engl*. **1994**, *33*, 2491 and references therein. (d) Khan, M. I.; Meyer, L. M.; Haushalter, R.; Zubieta, J.; Schweitzer, A.; Dye, J. L. *Chem. Mater*. **1996**, *8*, 43.
(8) Khan, M. I.; Zubieta, J. In *Early Transition Metal Clusters With* Π*-Donor Ligands*; Chisholm, M. H., Ed.; VCH: New York, 1995.
(9) Khan, M. I.; Zubieta, J. In *Prog. Inorg. Chem*. **1996**, *43*; 1−149.
(10) Zubieta, J. *Comments Inorg. Chem*. **1994**, *16*, 153.
(11) Chen, Q.; Zubieta, J. *Coord. Chem. Rev.* **1992**, *114*, 107.
(12) Eriksen, K. M.; Nielsen, K.; Fehrmann, R. *Inorg. Chem.* **1996**, *35*, 480 and references therein.
(13) Richter, K.-L.; Mattes, R. *Inorg. Chem*. **1991**, *30*, 4367 and references therein.
(14) Chang, Y.-D.; Chen, Q.; Khan, M. I.; Salta, J.; Zubieta, J. *J. Chem. Soc., Chem. Commun*. **1993**, 1872.
(15) Daniels, L. M.; Murrilo, C. A.; Rodriguez, K. G. *Inorg. Chim. Acta* **1995**, *229*, 27.
(16) Munno, G. D.; Bazzicalupi, C.; Faus, J.; Lloret, F.; Julve, M. *J. Chem. Soc., Chem. Commun*. **1994**, 1879.

S0020-1669(97)00971-3 CCC: $15.00 
Published on Web 01/12/1998

superacids $M_xO_y/SO_4$ (M = Ti, Zr, Fe) and their catalytic properties.[20] Recent modeling studies of the compositions of transition metal compounds of tetrahedral anions underline the potential of $SO_4^{2-}$ for synthesizing new inorganic materials constructed from oxometalate−sulfate building units.[21]

We are currently exploring the hydrothermal synthesis of oxovanadium−sulfate phases incorporating organic molecules and ions as structural buttresses. We believe that simple coordination compounds of vanadium and appropriate sources of $SO_4^{2-}$ are promising precursors to provide suitable building blocks for generating extended $M/O/SO_4^{2-}$ structures. By adopting this general strategy and exploiting the efficiency of the hydrothermal synthetic technique, we have now been able to prepare and isolate, in 70% yield, X-ray-quality crystals of a new solid: $[V_2O_2(OH)_2(SO_4)(2,2'\text{-bpy})_2]$ (**1**). This report describes the synthesis and characterization of **1** by complete single-crystal X-ray structure analysis, elemental analysis, manganometric titration, FT-IR spectroscopy, TGA, and variable-temperature magnetic susceptibility measurements.

## Experimental Section

**Materials.** All chemicals used during the course of this investigation were of reagent grade. These were used as received from the commercial source (Aldrich).

**Methods.** The IR spectrum (KBr Pellet; 4000−400 $cm^{-1}$) was recorded on a Paragon 1000 FT-IR spectrophotometer. The magnetic susceptibility data were recorded on a 34.40 mg crystalline sample of **1** over the 2−300 K temperature region using a Quantum Design MPMS-5S SQUID susceptometer. Measurement and calibration techniques have been reported elsewhere.[22] The temperature-dependent magnetic data were measured at a magnetic field of 1000 G. Thermogravimetric analysis was performed on a Perkin-Elmer 7 Series thermal analysis system by heating (10 °C/min) 6.452 mg of the sample under nitrogen atmosphere in the temperature range 30−550 °C. Titration of reduced vanadium ($V^{IV}$) sites in the compound was performed on a Mettler Toledo DL12 titrator using dilute acidic (1.8 N $H_2SO_4$) solutions of **1** and $KMnO_4$ solution ($7.6511 \times 10^{-3}$ M).

**Synthesis of $[V_2O_2(OH)_2(SO_4)(2,2'\text{-bpy})_2]$, 1.** The reaction was carried out in a 23 mL Parr Teflon-lined acid digestion bomb, heated in a Thermolyne programable electric furnace. A mixture of vanadyl acetylacetonate ($VO(acac)_2$), $Na_2SO_4$, 2,2′-bipyridine, and $H_2O$ in the molar ratio 1:3.33:3.33:92.60 was placed in a 23 mL Parr Teflon-lined autoclave which was subsequently heated for 48 h inside an electric furnace maintained at 160 °C. After the autoclave was cooled at room temperature for 4 h, brown crystals were filtered from the mother liquor, carefully washed with cold water, and dried in air at room temperature (yield = 70% based on vanadium).

Selected IR bands (1300−500 $cm^{-1}$ region): 1214 (vs), 1176 (w), 1159 (w), 1102 (vs), 1058 (w), 1019 (vs), 1007 (vs), 976 (vs), 970 (vs), 951 (vs), 783 (m), 771 (vs), 736 (vs), 668 (s), 663 (s), 596 (w), 535 (m).

**X-ray Structure Analysis.** The structure of **1** was determined from single-crystal X-ray diffraction data collected on a Siemens P4/CCD diffractometer (graphite-monochromatized Mo Kα radiation; $\lambda$ = 0.710 73 Å). A yellow-brown crystal (0.30 × 0.30 × 0.10 mm) of **1** was mounted on a glass fiber and centered. The unit cell parameters were obtained at 133(2) K on the basis of 6712 peaks ($3° \le \theta \le 25°$). A total of 8237 reflections ($2.10° \le \theta \le 25.82°$) were collected, of which 3078 unique reflections were used for structural elucidation. The data collection nominally covered a hemisphere of reciprocal space using $\phi$ rotation frames collected at 0.3° increments in $\phi$ for 30 s per frame. The crystal-to-detector distance was 5.26 cm. Coverage of the unique data set is over 89% complete to at least 25° in $\theta$. Crystal decay was estimated by comparing common intensities at the start and end of data collection and found to be negligible.

**Table 1.** Crystallographic Data for **1**

| | |
|---|---|
| empirical formula: $C_{20}H_{18}N_4O_8SV_2$ | fw: 576.32 |
| $a$ = 11.7937(2) Å | space group: $P2_1/n$ (No. 14) |
| $b$ = 12.1161(3) Å | $T$ = −140 °C |
| $c$ = 15.5763(2) Å | $\lambda$ = 0.710 73 Å |
| $\beta$ = 93.750(2)° | $\rho_{calcd}$ = 1.724 g $cm^{-3}$ |
| $V$ = 2220.99(7) Å | $\mu$ = 9.93 $cm^{-1}$ |
| $Z$ = 4 | $R^a$ = 0.049 |
| | $R_w{}^b$ = 0.128 |

$^a R = \sum||F_o| - |F_c||/\sum|F_o|$. $^b R_w = [\sum w(F_o^2 - F_c^2)^2/\sum w(F_o^2)^2]^{1/2}$.

All data were corrected for absorption on the basis of $\varphi$-scan profiles. The structure was solved in monoclinic space group $P2_1/n$ (No. 14) by direct methods and refined on $F^2$ by full-matrix least-squares techniques. At convergence, R1 equals to 0.0494 and the goodness-of-fit on $F^2$ is 1.221. Data collection,[23] data reduction,[24] and structure solution, refinement, and graphics[25] were done by use of the Siemens program packages. Neutral-atom scattering factors were taken from ref 26. Summaries of the crystal data and details concerning the intensity data collection and structure refinement are given in Table 1; full details have been deposited in the Supporting Information.

## Results and Discussion

The hydrothermal reaction of $VO(acac)_2$, $Na_2SO_4$, 2,2′-bipyridine, and $H_2O$ in the molar ratio 1:3.33:3.33:92.60 at 160 °C under autogenous pressure for 48 h yielded brown crystals of **1** in 70% yield. The mother liquor was allowed to remain at room temperature for several days to give a very small quantity of **1** and an amorphous off-white solid exhibiting IR absorption bands attributable to 2,2′-bipyridine, which was not further characterized. Other reactions with the same starting materials in different molar ratios and/or different reaction times produced **1** in reduced yield. Crystals of **1**, stable in air, were analyzed satisfactorily for the composition $C_{20}H_{18}N_4SO_8V_2$. The crystals are slightly (5−12 mg/100 mL) soluble in water, acetonitrle, DMSO, and methylene chloride.

The deep color of **1** is indicative of the reduced vanadium sites. This was confirmed by the manganometric titration where the number of reduced ($V^{IV}$) centers in the compound was determined by titrating it against standardized $KMnO_4$ solution. The result of the titration showed two $V^{IV}$ centers per molecule of **1**. This is consistent with the results of the magnetic susceptibility measurements (*vide infra*).

The infrared spectrum of **1** exhibits, besides 2,2′-bipyridine bands, very strong bands in 980−950 $cm^{-1}$ region characteristic of $\nu$(V═O). The multiple strong features in 1250−1000 $cm^{-1}$ region are attributable to the $\mu_2$-$SO_4^{2-}$ group spanning two vanadium(IV) centers. $\nu_1(SO_4^{2-})$ appears at 1007 $cm^{-1}$. The strong splitting of the $\nu_3(SO_4^{2-})$ bands (1214−1017 $cm^{-1}$ region) is indicative of the significant deformation of the $SO_4^{2-}$ ion from ideal tetrahedral geometry[12]—which has been confirmed by the crystal structure determination. Other low-energy bands, due to $\nu_2(SO_4^{2-})$, $\nu$(V−O−S), $\nu$(V−O−V), etc., are present in their characteristic region below 800 $cm^{-1}$. The

(17) Heerman, L.; Nyen, H. V.; D'Olieslager, W. *Inorg. Chim. Acta* **1996**, *244*, 191.
(18) Nielson, K.; Fehrmann, R.; Eriksen, K. M. *Inorg. Chem.* **1993**, *32*, 4825.
(19) Richter, K.-W.; Mattes, R. *Z. Anorg. Allg. Chem.* **1992**, *611*, 158.
(20) Lu, G. *Appl. Catal.* **1995**, *133*, 11.
(21) Lazoryak, B. I. *Russ. Chem. Rev.* (*Engl. Transl.*) **1996**, *65*, 287.
(22) O'Connor, C. J. *Prog. Inorg. Chem.* **1982**, *29*, 203.
(23) *SMART Software Reference Manual*; Siemens Analytical X-ray Instruments: Madison, WI, 1994.
(24) *SAINT Version 4 Software Reference Manual*; Siemens Analytical X-ray Instruments: Madison, WI, 1995.
(25) Sheldrick, G. M. *SHELXTL Version 5 Reference Manual*; Siemens Analytical X-ray Instruments: Madison, WI, 1994.
(26) *International Tables for Crystallography*; Kluwer: Boston, MA, 1995; Vol. C, Tables 6.1.1.4, 4.2.6.8, and 4.2.4.2.

**Table 2.** Atomic Coordinates and Equivalent Isotropic Displacement Parameters (Å$^2$) for **1**

| | *x* | *y* | *z* | *U*(eq)[a] |
|---|---|---|---|---|
| V(1A) | 0.52876(7) | 0.90520(7) | 0.56429(5) | 0.0132(2) |
| V(1B) | 0.62187(7) | 0.53085(7) | 0.47755(5) | 0.0142(2) |
| S(1) | 0.74699(10) | 0.76670(11) | 0.50721(7) | 0.0128(3) |
| O(1) | 0.6667(3) | 0.8038(3) | 0.5745(2) | 0.0158(8) |
| O(2) | 0.6855(3) | 0.6836(3) | 0.4494(2) | 0.0163(8) |
| O(3) | 0.8480(3) | 0.7181(3) | 0.5511(2) | 0.0187(8) |
| O(4) | 0.7738(3) | 0.8622(3) | 0.4534(2) | 0.0171(8) |
| O(1A) | 0.4354(3) | 1.0415(3) | 0.5491(2) | 0.0159(8) |
| O(2A) | 0.4324(3) | 0.8110(3) | 0.5490(2) | 0.0176(8) |
| O(1B) | 0.4854(3) | 0.5950(3) | 0.5210(2) | 0.0179(8) |
| O(2B) | 0.7077(3) | 0.5016(3) | 0.5589(2) | 0.0204(8) |
| N(1A) | 0.5081(3) | 0.9020(4) | 0.7005(3) | 0.0166(9) |
| C(2A) | 0.4278(4) | 0.8368(5) | 0.7333(3) | 0.0198(12) |
| C(3A) | 0.4085(4) | 0.8358(5) | 0.8201(3) | 0.0232(12) |
| C(4A) | 0.4724(4) | 0.9035(5) | 0.8756(3) | 0.0229(12) |
| C(5A) | 0.5540(4) | 0.9713(5) | 0.8434(3) | 0.0219(12) |
| C(6A) | 0.5700(4) | 0.9689(4) | 0.7550(3) | 0.0152(11) |
| C(7A) | 0.6558(4) | 1.0390(4) | 0.7151(3) | 0.0161(11) |
| C(8A) | 0.7264(4) | 1.1131(5) | 0.7610(3) | 0.0212(12) |
| C(9A) | 0.8037(4) | 1.1739(5) | 0.7168(3) | 0.0239(12) |
| C(10A) | 0.8087(4) | 1.1595(5) | 0.6290(3) | 0.0225(12) |
| C(11A) | 0.7355(4) | 1.0848(5) | 0.5874(3) | 0.0190(12) |
| N12A) | 0.6594(3) | 1.0254(4) | 0.6289(3) | 0.0159(9) |
| N(1B) | 0.7276(3) | 0.4398(4) | 0.3937(3) | 0.0162(9) |
| C(2B) | 0.8138(4) | 0.3771(5) | 0.4278(3) | 0.0192(11) |
| C(3B) | 0.8843(4) | 0.3156(5) | 0.3785(3) | 0.0235(13) |
| C(4B) | 0.8656(4) | 0.3194(5) | 0.2898(3) | 0.0250(13) |
| C(5B) | 0.7762(4) | 0.3818(5) | 0.2536(3) | 0.0222(12) |
| C(6B) | 0.7073(4) | 0.4411(5) | 0.3071(3) | 0.0169(11) |
| C(7B) | 0.6059(4) | 0.5052(4) | 0.2748(3) | 0.0169(11) |
| C(8B) | 0.5707(4) | 0.5104(5) | 0.1873(3) | 0.0202(12) |
| C(9B) | 0.4722(4) | 0.5691(5) | 0.1634(3) | 0.0219(12) |
| C(10B) | 0.4119(4) | 0.6195(5) | 0.2268(3) | 0.0221(12) |
| C(11B) | 0.4537(4) | 0.6105(5) | 0.3125(3) | 0.0183(11) |
| N(12B) | 0.5488(3) | 0.5544(4) | 0.3368(3) | 0.0147(9) |

[a] *U*(eq) is defined as one-third of the trace of the orthogonalized $\mathbf{U}_{ij}$ tensor.

intensities and positions of these spectral bands correspond to the observed values in the IR spectra of $K_6[(VO)_4(SO_4)_8]$,[12] $K[VO_2(SO_4)(H_2O)_2]\cdot H_2O$,[13] and related compounds containing $\mu_2$-$SO_4^{2-}$ ligands.[14]

The thermogravimetric analysis of **1** indicates no noticeable weight loss up to just below 300 °C. The thermogram curve records weight loss in the temperature range 300−390 °C corresponding to the liberation of a water molecule and decomposition of sulfate into sulfur oxides. The infrared spectrum of the green species obtained from heating **1** up to 395 °C shows that the organic part is still present. Further heating results in further decrease in weight in the temperature range 450−525 °C, corresponding to the decomposition of both 2,2′-bipyridine ligands (∼54% weight) into gaseous products. A constant weight plateau in the temperature range 525−550 °C suggests the possible formation of a stable reduced vanadium oxide phase, $V_xO_y$. The observed total weight loss (∼71%) corresponds to the complete decomposition of sulfate and 2,2′-bipyridine ligands and liberation of a molecule of water. This is further corroborated by the infrared spectral studies of the residue left after the thermogrametric analysis. The IR bands due to the sulfate and 2,2′-bipyridine ligands disappeared from the IR spectrum of the black residue, which now exhibits features at 998 (m), 743 (vs), and 537 cm$^{-1}$. The differential thermogram reveals that, like the liberations of water and sulfur oxides, the decompositions of both organic ligands also proceed almost simultaneously. While heating beyond 550 °C does not show any appreciable weight loss up to 1000 °C, it results in a bluish-purple material with medium-intensity IR bands below 1000 cm$^{-1}$. The color and the IR spectrum of the latter residue differ significantly from those of common reduced vanadium oxides: VO, $V_2O_3$, and $V_2O_4$.

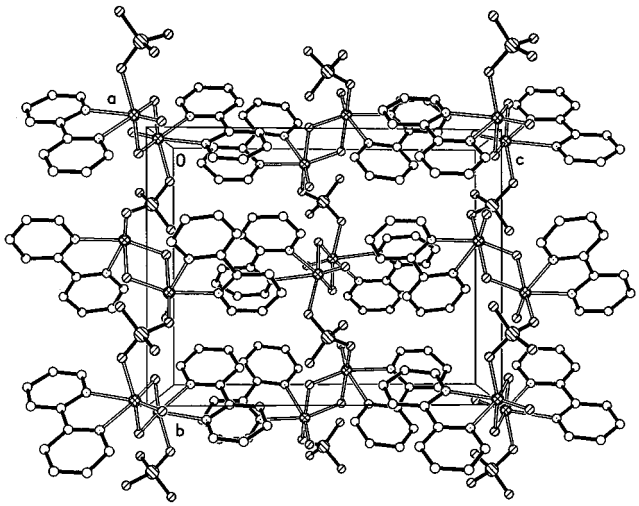


**Figure 1.** View of the packing of $[V_2O_2(OH)_2(SO_4)(2,2'\text{-bpy})_2]$ (**1**) along the *a* axis showing the ribbons of $[\{V_2(OH)_2\}-\mu_2\text{-}SO_4-\{V_2(OH)_2\}SO_4]$ composed of pairs of edge-sharing V(IV) octahedra and $SO_4^{2-}$ tetrahedra with organic (2,2′-bipyridine) ligands penetrating the interchain regions.

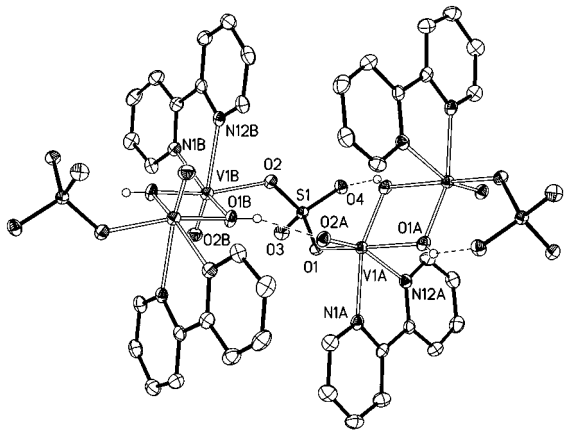


**Figure 2.** Perspective drawing showing the $\mu_2$-$SO_4$-bridged dinuclear building-block units in the structure of $[V_2O_2(OH)_2(SO_4)(2,2'\text{-bpy})_2]$ (**1**). The intrachain hydrogen-bonding pattern is also illustrated. Displacement ellipsoids are drawn at the 50% probability level. Bipyridine hydrogens are not shown.

Table 1 contains the X-ray crystallographic data for **1**. Atomic coordinates and bond lengths and angles are listed in Tables 2 and 3, respectively. The X-ray structural analysis of **1** revealed an extended structure (Figure 1) composed of the building-block units shown in Figure 2. The structure of **1** may be viewed as ribbons constructed from infinite zigzag inorganic chains, $[-\{V_2O_2(OH)_2\}-\mu_2\text{-}SO_4-\{V_2O_2(OH)_2\}SO_4-]_\infty$, incorporating 2,2′-bpyridine ligands. The neutral inorganic chains are composed of pairs of vanadium(IV) octahedra, defined by $\{V(O_2N_2)-\mu_2\text{-}(OH)_2-\mathbf{V}(O_2N_2)\}$ and fused through a common edge, which are linked by sulfate tetrahedra through octahedral−tetrahedral corner sharing as shown in Figure 3. The organic backbone of 2,2′-bipyridine ligands extend sideways from either face of the inorganic ribbons, penetrating the interchain regions that separate the adjacent parallel inorganic chains (Figure 1). Each organic stack is, in turn, bound by two consecutive stacks of inorganic chains.

The octahedral geometry around each vanadium ion is defined by $\{VO_2(OH)_2N_2\}$ with each $V^{IV}$ center coordinated to a

**Table 3.** Selected Bond Lengths (Å) and Angles (deg) for **1**

| | | | |
|---|---|---|---|
| V(1A)−O(2A) | 1.618(4) | V(1A)−O(1A)#1 | 1.953(3) |
| V(1A)−O(1A) | 1.990(3) | V(1A)−O(1) | 2.037(3) |
| V(1A)−N(1A) | 2.152(4) | V(1A)−N(12A) | 2.303(4) |
| V(1A)−V(1A)#1 | 3.094(2) | V(1B)−O(2B) | 1.608(4) |
| V(1B)−O(1B) | 1.948(3) | V(1B)−O(1B)#2 | 1.982(4) |
| V(1B)−O(2) | 2.055(4) | V(1B)−N(1B) | 2.165(4) |
| V(1B)−N(12B) | 2.320(4) | V(1B)−V(1B)#2 | 3.094(2) |
| S(1)−O(3) | 1.459(4) | S(1)−O(4) | 1.475(4) |
| S(1)−O(2) | 1.505(4) | S(1)−O(1) | 1.525(3) |
| O(1A)−V(1A)#1 | 1.953(3) | O(1B)−V(1B)#2 | 1.982(4) |
| O(2A)−V(1A)−O(1A)#1 | 106.9(2) | O(2A)−V(1A)−O(1A) | 101.0(2) |
| O(1A)#1−V(1A)−O(1A) | 76.63(14) | O(2A)−V(1A)−O(1) | 97.8(2) |
| O(1A)#1−V(1A)−O(1) | 92.91(13) | O(1A)−V(1A)−O(1) | 160.5(2) |
| O(2A)−V(1A)−N(1A) | 90.5(2) | O(1A)#1−V(1A)−N(1A) | 160.6(2) |
| O(1A)−V(1A)−N(1A) | 92.0(2) | O(1)−V(1A)−N(1A) | 93.08(14) |
| O(2A)−V(1A)−N(12A) | 162.6(2) | O(1A)#1−V(1A)−N(12A) | 90.5(2) |
| O(1A)−V(1A)−N(12A) | 82.9(2) | O(1)−V(1A)−N(12A) | 80.76(14) |
| N(1A)−V(1A)−N(12A) | 72.3(2) | O(2A)−V(1A)−V(1A)#1 | 107.85(13) |
| O(1)−V(1A)−V(1A)#1 | 129.68(10) | N(1A)−V(1A)−V(1A)#1 | 128.15(13) |
| N(12A)−V(1A)−V(1A)#1 | 85.72(11) | O(3)−S(1)−O(4) | 112.6(2) |
| O(3)−S(1)−O(2) | 111.0(2) | O(4)−S(1)−O(2) | 107.3(2) |
| O(3)−S(1)−O(1) | 108.8(2) | O(4)−S(1)−O(1) | 109.0(2) |
| O(2)−S(1)−O(1) | 108.2(2) | S(1)−O(1)−V(1A) | 130.8(2) |
| S(1)−O(2)−V(1B) | 130.0(2) | V(1A)#1−O(1A)−V(1A) | 103.37(14) |
| V(1B)−O(1B)−V(1B)#2 | 103.9(2) | | |

[a] Symmetry transformations: (#1) $1-x, 2-y, 1-z$; (#2) $1-x, 1-y, 1-z$.

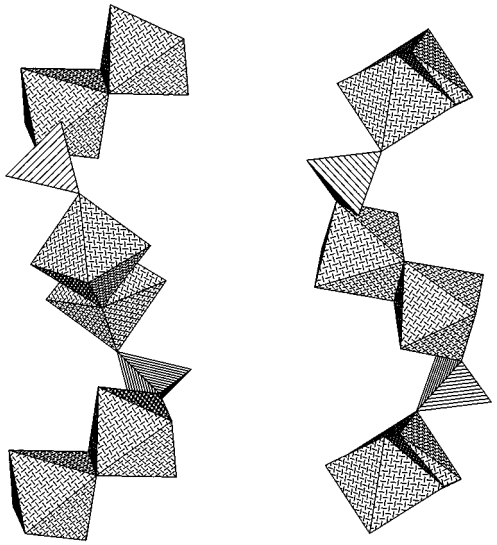

**Figure 3.** Polyhedral representation of the infinite chains, $[-\{V_2O_2(OH)_2\}-\mu_2\text{-}SO_4-\{V_2O_2(OH)_2\}SO_4-]_\infty$, showing pairs of edge-sharing octahedra $\{V(O_4N_2)\}$ joined by sulfate tetrahedra through octahedral−tetrahedral corner sharing.

terminal oxo group, two $\mu_2$-OH groups, two nitrogen donor atoms from a chelating 2,2′-bipyridine ligand, and an oxygen donor atom from a $\mu_2$-$SO_4$2- ligand. This arrangement generates a four-membered, $-V^{IV}-O(H)-V^{IV}-O(H)-$, rhombus-shaped metallacycle with V−O(H)−V and O(H)−V−O(H) bond angles 103.9(2)−103.37(14) and 76.1(2)−76.63(14)°, respectively. The $V^{IV}-V^{IV}$ distance is 3.094(2) Å. All four internal V−($\mu$-O)-(H) distances in the {V− ($\mu_2$-OH)$_2$−V} moiety, found to be approximately equal (1.948(3)−1.990(3)Å), are comparable to other V−($\mu$-O)(H) distances reported, earlier, by us[27] and others, and significantly different from the literature-reported V−($\mu$-O) and V−($\mu$-O)(H$_2$) distances given in Table 4. This, along with the results of the valence sum calculations (Table 4), leads to the unambiguous identification of both of the oxygens (O(1A) and O(1B)) as hydroxy groups.

While the {(OV)$_2$(OH)$_2$}core has been observed earlier also,[32] the $\{O{=}V^{IV}(\mu_2\text{-}OH)_2V^{IV}{=}O\}$ core in **1** represents a unique structural feature of the $V^{IV}$/O/$SO_4$/2,2′-bpy system. The two terminal oxo groups adopt an *anti* configuration with one $V-O_{terminal}$ vector pointing above and the other pointing below the plane of the $V^{IV}(\mu_2\text{-}OH)_2V^{IV}$ rhombus ($V-O_{terminal}$ bond lengths = 1.618(4), 1.608(4) Å; $O_{terminal}-V-V$ angles = 107.85(13), 108.35(13)°). The 2,2′-bipyridine is present in an usual chelating bidentate mode, forming a five-membered ring defined by −V−N−C−C−N− with V−N bond lengths of 2.152(4)−2.165(4) and 2.303(4)−2.320(4) Å and N−V−N bond angles of 72.3(2) (N(1A)−V(1A)−N(12A)) and 71.7(2)° (N(1B)−V(1B)−N(12B)). The metrical parameters are comparable to those observed in the molecular compound V(2,2′-bipy)$_2$$SO_4$[15] and the solid $[VO(VO_3)_6(VO(2,2'\text{-}bpy)_2)_2]$.[33] The chelate ring defined by V(1A)−N(1A)−C−C−N(12A) (Figure 2), 2,2′-bpyridine rings, and the terminal oxo group on the vanadium center are in a plane almost perpendicular to the plane of the $\{V^{IV}-(\mu_2\text{-}OH)_2-V^{IV}\}$ rhombus.

The $SO_4^{2-}$ ligand adopts a $\mu_2$-bridging mode linking two $V^{IV}$ centers (Figure 2), one from each of the two nearest $\{V^{IV}-(\mu_2\text{-}OH)_2-V^{IV}\}$ motifs, through two of its oxygens, O(1) and O(2), with V(1A)−O(1) and V(1B)−O(2) bond lengths of 2.037(3) and 2.055(4) Å, respectively. These distances compare well to the corresponding distances involving $V^{IV}$ centers in

(27) Khan, M. I.; Chang, Y.-D.; Chen, Q.; Salta, J.; Lee, Y.-S.; O'Connor, C. J.; Zubieta, J. *Inorg. Chem*. **1994**, *33*, 6340 and references therein.
(28) Brown, I. D. In *Structure and Bonding in Crystals*; O'Keefe, M., Navrotsky, A., Eds.; Academic Press: New York, 1981; Vol. II, p 1.
(29) (a) Knopp, P.; Wieghardt, K.; Nuber, B.; Weiss, J.; Sheldrick, W. S. *Inorg. Chem*. **1990**, *29*, 363. (b) Neves, A.; Wieghardt, K.; Nuber, B.; Weiss, J. *Inorg. Chim. Acta* **1988**, *150*, 183.
(30) Müller, A.; Rohlfing, R.; Krickemeyer, E.; Bögge, H. *Angew. Chem., Int. Ed. Engl*. **1993**, *32*, 909.
(31) Khan, M. I.; Chang, Y.-D.; Chen, Q.; Salta, J.; Lee, Y.-S.; O'Connor, C. J.; Zubieta, J. *Inorg. Chem*. **1994**, *33*, 6340.
(32) (a) Weiss, A.; Riegler, E.; Alt, I.; Robl, C. *Z. Naturforsch*, **1986**, *41B*, 18. (b) Robl, C.; Weiss, A. *Z. Naturforsch*, **1986**, *41B*, 1341. (c) Petite, J. F.; Trombe, J. C.; Gleizes, A.; Galy, J. *C. R. Acad. Sci., Ser. 2* **1987**, *304*, 1117.
(33) Huan, G.; Johnson, J. W.; Jacobson, A. J. *J. Solid State Chem*. **1991**, *91*, 4937.

**Table 4.** Results of Valence Sum Calculations and Observed V−$\mu_2$-O(H), V−$\mu_2$-O, and V−$\mu_2$-O($H_2$) Bond Distances (Å) in Selected Vanadium Compounds

| compound | V−O−V | $\sum S_i$[a] | V−O(H)−V | $\sum S_i$ | V−O($H_2$)−O | $\sum S_i$ | ref |
|---|---|---|---|---|---|---|---|
| $[V_2O_2(OH)_2([9]aneN_3)_2]^{2+}$ | | | 1.969(5) | 1.25 | | | 29 |
| $Na[V_2O_2(OH_2)_3(OH)_2(C_4O_4)_2]$ | | | 1.97(1) | 1.25 | 2.38(1) | | 30 |
| $NH_4[V_2O_2(OH_2)_3(OH)(C_4O_4)_2]\cdot H_2O$ | | | 1.98(2) | 1.21 | 2.40(2) | 0.35 | 31 |
| $Bu_4N[V_2O_3(OH_2)_3(C_4O_4)_2]\cdot 3H_2O$ | 1.822(7) | 1.93 | | | 2.460(6) | 0.30 | 31 |
| $(Bu_4N)_4[V_4O_6(OH_2)_4(C_4O_4)_5]\cdot 6H_2O$ | 1.82(1) | 1.94 | | | | | 31 |
| $[V_2O_2(OH)_2(SO_4)(2,2'\text{-bpy})_2]$ | | | 1.968(4) | 1.15 | | | this work |

[a] Valence sums in valence units, calculated according to ref 28. No hydrogen atom contributions.

the fully reduced cluster $[Bu^n_4N]_2[V_4O_4(H_2O)_2(SO_4)_2\{(OCH_2)_3CCH_2CH_3\}_2]$ reported by us[14] and in the mixed-valence species $K_6[(VO)_4(SO_4)_8]$[12] and are, in general, slightly longer than the corresponding values involving $V^V$ sites (e.g., in $M[VO(SO_4)_2]$ (M = K, $NH_4$),[19] $[V_2O_3(SO_4)_2]$,[19] $K[VO_2(SO_4)(H_2O)]$,[13] and $K[VO_2(SO_4)(H_2O)_2]\cdot H_2O$[13] (sulfate as $\mu_2$-$SO_4$) and in $Cs_4[(VO)_2O(SO_4)_4]$[18] ($SO_4^{2-}$ as a bidentate chelating ligand)).

The O(1)−V(1A)−O(1A) and O(2)−V(1B)−O(1B)#2 angles are 160.5(2) and 159.59(14)°, respectively. The S(1)−O(1)−V(1A) and S(1)−O(2)−V(1B) angles are 130.8(2) and 130.0(2)°, respectively. These are not different from the corresponding values observed in $K[VO_2(SO_4)(H_2O)]$.[13] The S(1)−O(1) and S(1)−O(2) bonds are longer than the bonds to noncoordinated oxygens. The latter two bonds, S(1)−O(3) and S(1)−O(4), span the widest angle, O(3)−S(1)−O(4) = 112.6(2)°, in the $SO_4^{2-}$ tetrahedron. The overall geometry around sulfur is a distorted tetrahedron. The planes of the two nearest $\{V^{IV}-(\mu_2\text{-}OH)_2-V^{IV}\}$ motifs, linked by $\mu_2$-$SO_4$, are significantly twisted with respect to each other, resulting in the zigzag feature of the chain. The intrachain hydrogen bondings in **1** are characterized by short O(2A)···H−(O(1B)) (1.953(5) Å) and O(4)···H−(O(1A)#1) (1.895(5) Å) distances (Figure 2) due to the restricted geometries of the rhombuses; the corresponding O···O distances are 2.732(5) Å (O(2A)···O(1B)) and 2.728(5) Å (O(4)···O(1A)#1). The bond angles O(2A)···H−O(1B) and O(4)···H−O(1A)#1 are 157.08(14) and 149.93(14)°, respectively.

The temperature-dependent magnetic susceptibility data for **1** exhibit Curie−Weiss paramagnetism at high temperature ($T$ > 140 K) with the fitted parameters $C$ = 0.807 emu·K/mole, $\theta$ = −80.97 K, $g$ = 2.07, and TIP = 0.0087. The inverse magnetic susceptibility data are plotted in Figure 4 (inset) with the fitted curve. As shown in Figure 4, at lower temperature, the magnetic susceptibility exhibits a broad maximum consistent with short-range antiferromagnetic coupling. The magnetic data were analyzed in the vicinity of the maximum using a model that assumes coupling of two $S = {}^1/_2$ vanadium(IV) centers. The isotropic coupling of these two centers gives the following magnetic susceptibility equation:[34]

$$\chi = [Ng\mu_B{}^2/kT][2e^{2x}/(1 + 3e^{2x})] \quad (1)$$

where $x = J/kT$. The magnetic data also required correction using the molecular field approximation due to secondary interactions, either from interdimer coupling or from zero-field splitting of the $S = {}^1/_2$ multiplet. The secondary interactions were treated using the molecular field approximation[22] as follows:

$$\chi = \chi'/[1 - (2zJ'/Ng^2\mu_B{}^2)\chi'] \quad (2)$$

(34) Bleaney, B.; Bowers, K. D. *Proc. R. Soc. London* **1952**, *A214*, 451.

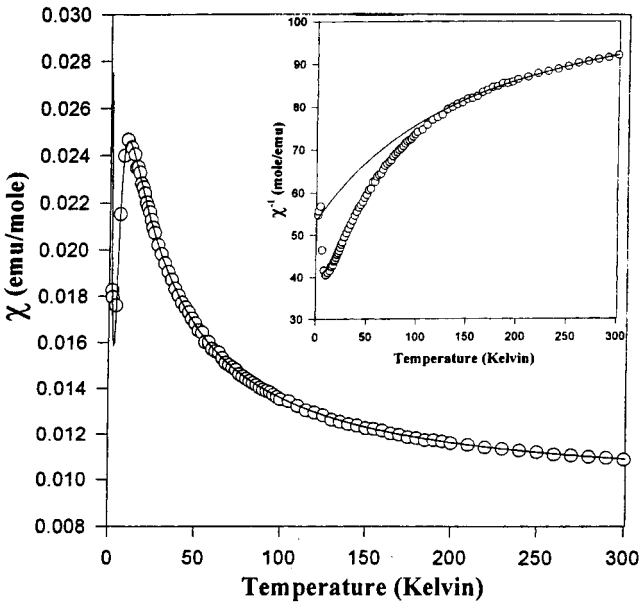


**Figure 4.** Magnetic susceptibility of **1** plotted as a function of temperature over the 1.7−300 K temperature region. The curve drawn through the data is the fit to the binuclear model as described in the text. The inset shows the inverse magnetic susceptibility of **1** plotted as a function of temperature over the 1.7−300 K temperature region. The line drawn through the data is the fit to the Curie−Weiss model as described in the text.

where $\chi'$ is the magnetic susceptibility of the material in the absence of the exchange field (eq 1) and $\chi$ is the molecular exchange field influenced magnetic susceptibility that is actually measured. The exchange field coupling parameter is $zJ'$, where $z$ is the number of exchange-coupled neighbors. The addition of the molecular field exchange correction resulted in a substantial improvement of the fit to the data. The magnetic susceptibilities of $Cs[(VO)_2(OH)(O_3PCH_2CH_2PO_3)]$ were fit to eq 1 corrected by eq 2 and gave the following parameters: $g$ = 2.00, $J/k$ = −9.15 K, $zJ'/k$ = −14.33, TIP = 0.0119, with 4% monomer impurities.

While there are few earlier reports on molecular compounds and solids with oxovanadate−sulfate motifs,[12−19] **1** represents a solid with a number of unique features. The structure of **1** contains inorganic ribbons composed of less commonly observed pairs of edge-sharing octahedra joined by $\{SO_4\}$ tetrahedra. Unlike the other known oxovanadosulfate solids containing "naked" inorganic structures, **1** provides an example of a V/O/$SO_4$-based material exhibiting solid state coordination chemistry by employing an organic ligand around the inorganic V/O/$SO_4$ backbone to saturate the coordination sphere of vanadium ions. Furthermore, **1** constitutes the first example of a vanadosulfate-based organic/inorganic solid containing all reduced vanadium(IV) centers.

The preparation and characterization of **1** appear to be a significant step toward further development of V/O/$SO_4$/L (L

= organic ligand) systems, providing possibilities for the synthesis of new molecular systems and solids by incorporating both inorganic and organic ligands around metal oxide cores. Since a large number of clusters and solid phases with layered and zeolitic structures have arisen from $V/O/PO_4$ systems, the chemistry of the $V/O/SO_4/L$ system is promising. While **1** is a neutral compound, the incorporation/encapsulation of organic and inorganic cations and structure-directing templates may result in the formation of different structures. These possibilities are currently under investigation in our laboratories. The high-yield synthesis of **1** further demonstrates the versatility of the hydrothermal methods for the efficient preparation of new materials with novel structural and topological features.

**Acknowledgment.** This work was supported by the Illinois Institute of Technology through an ERIF grant to M.I.K. D.P. acknowledges funds from the NSF (Grant CHE-9310428) and from the University of Wisconsin for the purchase of the X-ray instrument and computers. C.J.O. acknowledges support from DARPA (Grant MDA972-97-1-0003).

**Supporting Information Available:** Tables listing crystal data and structure refinement details, bond lengths and bond angles, anisotropic displacement parameters, hydrogen atom coordinates, and torsion angles for the structure of **1** (9 pages). Ordering information is given on any current masthead page.

IC970971O